iScience

CellPress
OPEN ACCESS

Article

Optimized *in vivo* multispectral bioluminescent imaging of tumor biology using engineered BRET reporters

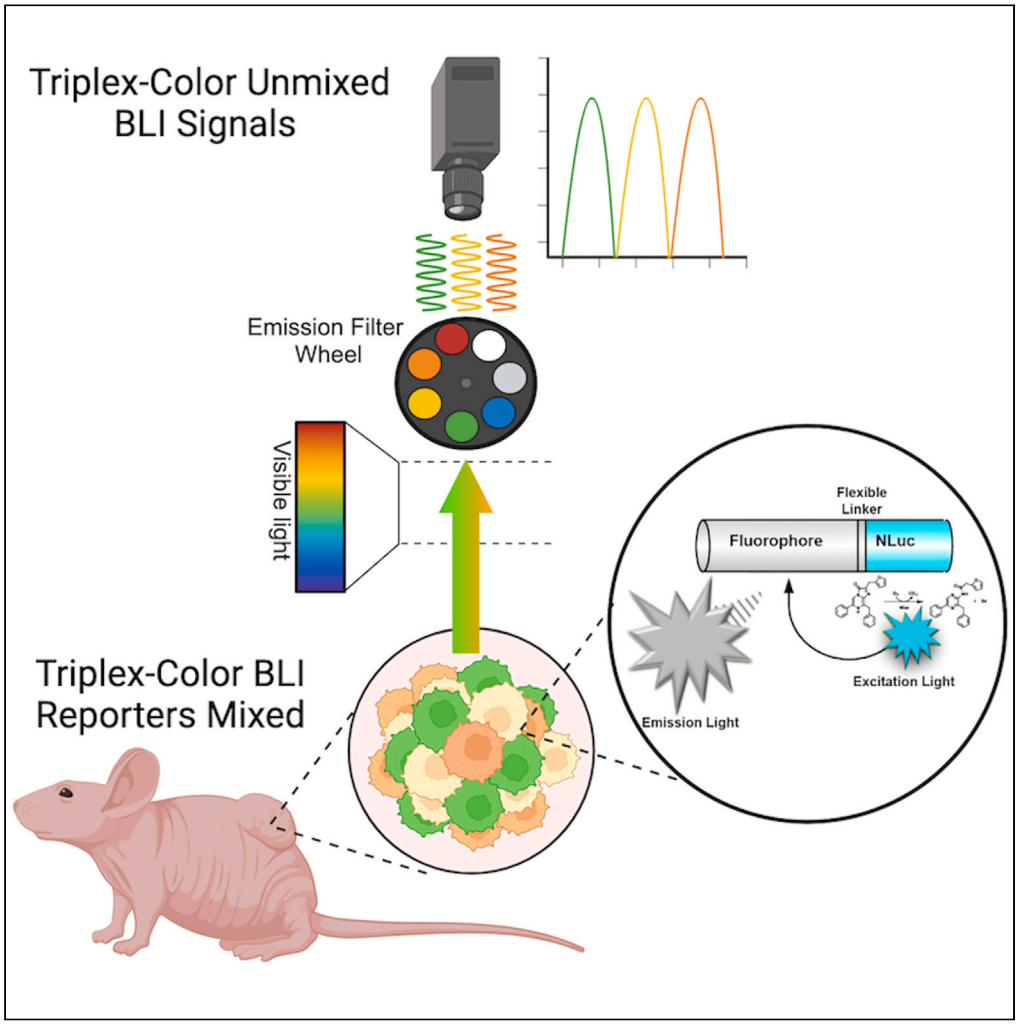

Bryan Labra, Kshitij Parag-Sharma, John J. Powers, ..., Caroline K. Brennan, Jennifer A. Prescher, Antonio L. Amelio

antonio.amelio@moffitt.org

Highlights

Library of epitope-tagged bioluminescence resonance energy transfer (BRET) reporters

Directly compared two orthologous nanoluciferase substrates *in vitro* and *in vivo*

Optimize both two- and three-color BLI in tumors using these BRET reporters

Labra et al., iScience 27, 110655
September 20, 2024
https://doi.org/10.1016/j.isci.2024.110655

iScience

CellPress
OPEN ACCESS

Article

Optimized *in vivo* multispectral bioluminescent imaging of tumor biology using engineered BRET reporters

Bryan Labra,[1] Kshitij Parag-Sharma,[2] John J. Powers,[3] Sonal Srivastava,[3] Joel R. Walker,[4] Thomas A. Kirkland,[4,5] Caroline K. Brennan,[6] Jennifer A. Prescher,[6,7,8] and Antonio L. Amelio[3,9,10,11,12,*]

SUMMARY

The ability to visualize and track multiple biological processes *in vivo* in real time is highly desirable. Bioluminescence imaging (BLI) has emerged as an attractive modality for non-invasive cell tracking, with various luciferase reporters enabling parallel monitoring of several processes. However, simultaneous multiplexed imaging *in vivo* is challenging due to suboptimal reporter intensities and the need to image one luciferase at a time. We report a multiplexed BLI approach using a single substrate that leverages bioluminescence resonance energy transfer (BRET)-based reporters with distinct spectral profiles for triple-color BLI. These luciferase-fluorophore fusion reporters address light transmission challenges and use optimized coelenterazine substrates. Comparing BRET reporters across two substrate analogs identified a green-yellow-orange combination that allows simultaneous imaging of three distinct cell populations *in vitro* and *in vivo*. These tools provide a template for imaging other biological processes *in vivo* during a single BLI session using a single reporter substrate.

INTRODUCTION

A multitude of imaging modalities with applications in pre-clinical animal models have emerged over the past century.[1] Notably, various optical imaging techniques that exploit the emission and detection of photons traveling through tissue have enabled observation at both the microscopic and macroscopic scales. Bioluminescence imaging (BLI) represents one such optical imaging modality that has been successfully adopted and refined for non-invasively monitoring molecular and cellular processes in living animals over extended timescales.[2,3] The success of BLI stems from the plethora of luciferase enzymes that have been discovered and optimized to emit photons within the visible light spectrum following catalysis of small-molecule substrates.[4,5] Moreover, the apparent absence of an endogenous bioluminescent signal within biologic tissues ensures a high signal-to-noise ratio, which contrasts with fluorescent imaging where significant tissue autofluorescence limits its utility *in vivo*. This ability to interrogate biological processes, as they occur in real time with high specificity and sensitivity, provides a unique opportunity to investigate three-dimensional spatial cues, multiple cell types acting in parallel, or other phenomena that can only be studied *in vivo*.

Tumorigenesis and progression is a complex, multi-parametric biologic process that requires interaction between, and crosstalk across, a milieu of cell types and signaling pathways.[6] This complexity offers a unique opportunity to exploit the benefits of BLI to visualize aspects of these processes to better understand the mechanistic underpinnings of this disease, albeit at lower spatial resolution compared to intravital imaging.[7,8] Notably, the selection of the luciferase used for these efforts is paramount given that auto-inactivation by enzymatic by-products can contribute to wide variability in the intensity and duration of photon output for some luciferases.[9] More importantly, harsh conditions such as hypoxia, low pH, and urea cycle dysregulation within tumor microenvironments can generally pose a significant obstacle to optimal performance of enzymes such as luciferases.[6,10–14] Identification of a mutant Oplophorus luciferase (NanoLuc) with improved properties to these

[1]Lineberger Comprehensive Cancer Center, UNC School of Medicine, The University of North Carolina at Chapel Hill, Chapel Hill, NC, USA
[2]Graduate Curriculum in Cell Biology & Physiology, Biological & Biomedical Sciences Program, UNC School of Medicine, The University of North Carolina at Chapel Hill, Chapel Hill, NC, USA
[3]Department of Tumor Microenvironment and Metastasis, H. Lee Moffitt Cancer Center & Research Institute, Tampa, FL 33612, USA
[4]Promega Biosciences, LLC, San Luis Obispo, CA, USA
[5]Promega Corporation, Madison, WI, USA
[6]Department of Chemistry, University of California, Irvine, Irvine, CA, USA
[7]Department of Pharmaceutical Sciences, University of California, Irvine, Irvine, CA, USA
[8]Department of Molecular Biology and Biochemistry, University of California, Irvine, Irvine, CA, USA
[9]Cancer Cell Biology Program, Lineberger Comprehensive Cancer Center, UNC School of Medicine, The University of North Carolina at Chapel Hill, Chapel Hill, NC, USA
[10]Department of Cell Biology and Physiology, UNC School of Medicine, The University of North Carolina at Chapel Hill, Chapel Hill, NC, USA
[11]Department of Head and Neck-Endocrine Oncology, H. Lee Moffitt Cancer Center & Research Institute, Tampa, FL 33612, USA
[12]Lead contact
*Correspondence: antonio.amelio@moffitt.org
https://doi.org/10.1016/j.isci.2024.110655

conditions[12] suggested that when coupled with optimized coelenterazine substrate analogs (e.g., furimazine), NanoLuc would be functional within the tumor microenvironment similar to that observed with other ATP-dependent firefly and click beetle or ATP-independent Renilla and Gaussia luciferases. However, the NanoLuc:furimazine spectral emission profile is largely restricted to short-wavelength blue light, which limits signal detection for *in vivo* BLI applications without further modification.[11,15]

Bioluminescence resonance energy transfer (BRET)-based optical reporters employing NanoLuc (e.g., LumiFluor reporters) have emerged as promising tools for monitoring tumorigenesis and responses to drug therapy using *in vivo* BLI.[15–18] These BRET molecules employ direct fusion of a donor NanoLuc moiety and a fluorescent protein acceptor, which consequently tunes the emission profile to longer wavelengths that penetrate tissues better. Despite the growing use of these BLI tools, they have been primarily used to track a single parameter *in vivo*. Recent studies have explored the feasibility of tracking multiple parameters with BLI,[19] but these efforts have been restricted to two parameters using spectrally resolved reporters that often depend on the sequential administration of distinct substrates.[2,20–24] Thus, the promise of tracking multiple processes in parallel remains challenging due to critical experimental limitations with currently available BLI tools and protocols, which restrict their appropriate implementation.

Herein, we leveraged a collection of BRET-based tools with distinct spectral emission profiles to perform direct comparisons between multiple triplex reporter combinations and identify an optimal multiplexed BLI approach for monitoring three independent parameters *in vivo*. Notably, this three-color combination only requires the administration of a single optimized substrate, which enabled rapid and reproducible imaging of heterogeneous tumor cell populations both *in vitro* and *in vivo*. These tools provide a proof-of-concept methodology that can be further adapted to perform simultaneous triplexed BLI analyses on a multitude of other biological processes *in vivo* during a single imaging session by administration of a single reporter substrate.

RESULTS

Spectral characterization of NanoLuc-based BRET reporters administered coelenterazine substrate analogs

The ability to effectively tune spectral emission outputs from luciferase donor moieties such as NanoLuc has led to a growing list of customizable BRET molecules with considerable flexibility in their optical reporter properties and suitability for *in vivo* applications (Table 1). To directly compare these reporter properties both *in vitro* and *in vivo*, we first generated a panel of epitope-tagged versions of available NanoLuc-based BRET molecules spanning the visible spectrum within a lentiviral format and validated their expression in stably selected cells (Figure 1A; Figure S1). Luminescence assays confirmed that shorter wavelength reporters with greater J(λ) overlap between donor NanoLuc and acceptor fluorophore (e.g., CeNLuc and GpNLuc relative to OgNLuc) produce ∼3-fold greater total light output (Figure 1B). Comparison of substrate-dependent light output (i.e., 20 μM furimazine [FZ] or 20 μM of its chemical ortholog fluorofurimazine [FFZ]) revealed that while total light output was nearly equivalent for GeNL and YeNL regardless of the substrate administered, there was a modest ∼1.5-fold increase for FFZ relative to FZ for the other BRET reporters tested (Figure 1B). Notably, the signals decayed at different rates when comparing the total light output produced by FFZ relative to FZ such that CeNLuc, CeNL, GpNLuc, and OeNL displayed ∼2-fold increase in decay and GeNL and YeNL had nearly equivalent decay rates, while OgNLuc displayed an opposite ∼2-fold decrease in signal decay from ∼25 min with FFZ down to ∼10 min with FZ (Figures 1C; Table 2; Figure S2).

Next, we evaluated the luminescent intensities produced by each reporter at their respective spectral peaks, rather than total luminescent output, when administered FZ versus FFZ. Spectral emission profiles spanning the 400–650 nm range were first generated *in vitro* using a monochromator-based approach (BioTek Cytation 5) at 5 nm resolution between readings and validated that each BRET reporter produces equivalent peak emission wavelengths, indicating that when compared to FZ, catalysis of the FFZ analog does not influence the BRET process and consequent BRET spectral profile (Figure 1D). Peak emission intensity, however, was modestly enhanced with FFZ compared to FZ (∼1.5- to ∼2-fold) for select reporters as expected based on results from the total light output assays (Figure 1B; Figure S3A). These reporters were then assessed using an industry standard pre-clinical optical imaging system that employs a CCD camera and filter-based approach (IVIS Spectrum), albeit at 20 nm resolution between readings and only spanning the 500–600 nm range. These assays confirmed observations made using the monochromator-based instrument such that each BRET reporter produces equivalent peak emissions, although only YeNL appears to display a significant ∼2-fold increase in photon output at 540 nm with FFZ substrate administration (Figure 1E; Figures S3B and S3C). These results indicate that peak emission values are consistent between the substrates evaluated and can therefore be used to inform strategies aimed at multiplexing the BRET reporters.

Optimization of BRET reporter combinations for multispectral imaging

To facilitate the design of multispectral imaging paradigms, we generated stable cell lines and determined the proliferation rates for each stable reporter cell line to ensure that differences in BLI measurements are not due to differences in cell growth (Figure S4). These cell growth assays confirmed that all the stable reporter cell lines retain normal growth rates as compared to the parental UM-HMC-1 parental cells. Optimal BRET reporter combinations composed of three colors were then predicted based on normalized emission spectra, and selections were made for each reporter (CeNLuc @ 500 nm, GpNLuc @ 520 nm, GeNL @ 540 nm, YeNL @ 560 nm, OeNL @ 580, and LumiScarlet @ 600 nm) where spectral separation was greatest and the amount of IVIS signal detected from within adjacent band-pass filter sets was minimal (Figure 2A; Table 1). Given the broad range of photons emitted, photons emanating from each BRET reporter overlapped and were detectable within band-pass filter sets of adjacent reporters. However, by resolving these signals using a spectral unmixing approach, five unique combinations were selected that minimize spectral overlap for further evaluation and included: (1) CeNLuc/GpNLuc/LumiScarlet, (2) CeNLuc/GeNL/OeNL, (3) GpNLuc/YeNL/LumiScarlet, (4) GpNLuc/YeNL/OeNL, and (5) GeNL/YeNL/LumiScarlet.

Table 1. BRET reporters derived using engineered versions of the *Oplophorus gracilirostris* luciferase

BRET reporter	Reporter color	Luciferase (em^{max})	Substrate(s)	Fluorophore (ex^{max}/em^{max})	Spectral Separation	Addgene (catalog #)	Reference(s)
CeNLuc	Blue	NanoLuc (460 nm)	FZ, FFZ, HFZ	mCerulean3 (433/475 nm)	15 nm	135933, 135933, 183036, 208838	Brennan et al.,[21]; Su et al.[22,a]
CeNL	Blue	NanoLuc (460 nm)	FZ, FFZ, HFZ	mTurquoise2 (434/475 nm)	15 nm	85199, 208839	Viviani[14,a]
GpNLuc	Green	NanoLuc (460 nm)	FZ, FFZ, HFZ	eGFP (488/509 nm)	49 nm	70185, 135935, 183037, 208840	Hall et al.,[12]; Brennan et al.,[21]; Su et al.[22,a]
GeNL	Green	NanoLuc (460 nm)	FZ, FFZ, HFZ	mNeonGreen (506/517 nm)	57 nm	85200, 208841	Viviani[14,a]
YeNL	Yellow	NanoLuc (460 nm)	FZ, FFZ, HFZ	Venus (515/528 nm)	68 nm	85201, 208849	Viviani[14,a]
OeNL	Orange	2x NanoLuc (460 nm)	FZ, FFZ, HFZ	mKO_K (551/563 nm)	103 nm	85202, 208850	Viviani[14,a]
OgNLuc	Orange	NanoLuc (460 nm)	FZ, FFZ, HFZ	LSSmOrange (437/572 nm)	112 nm	70186, 135936, 183038, 208851	Hall et al.,[12]; Brennan et al.,[21]; Su et al.[22,a]
Antares	Orange	NanoLuc (460 nm)	FZ, FFZ, HFZ	2x CyOFP1(497/589 nm)	129 nm	74279, 183049, 208852	Su et al.,[22]; Stowe et al.[23,a]
Antares2	Orange	teLuc (502 nm)	DTZ	2x CyOFP1(497/589 nm)	129 nm	100027, 208853	Taylor et al.[24,a]
LumiScarlet	Red	LumiLuc (440, 475, 525 nm)	pyCTZ, 6pyDTZ, 8pyDTZ	mScarlet-I (569/593 nm)	133 nm	126623, 183044, 208854	Schaub et al.,[15]; Su et al.[22,a]

em, emission; ex, excitation; nm, nanometer; FZ, furimazine; FFZ, fluorofurimazine; HFZ, hydrofurimazine; DTZ, diphenylterazine; pyCTZ, pyridylcoelenterazine; 6pyDTZ and 8pyDTZ, pyridyldiphenylterazine.
[a]This paper.

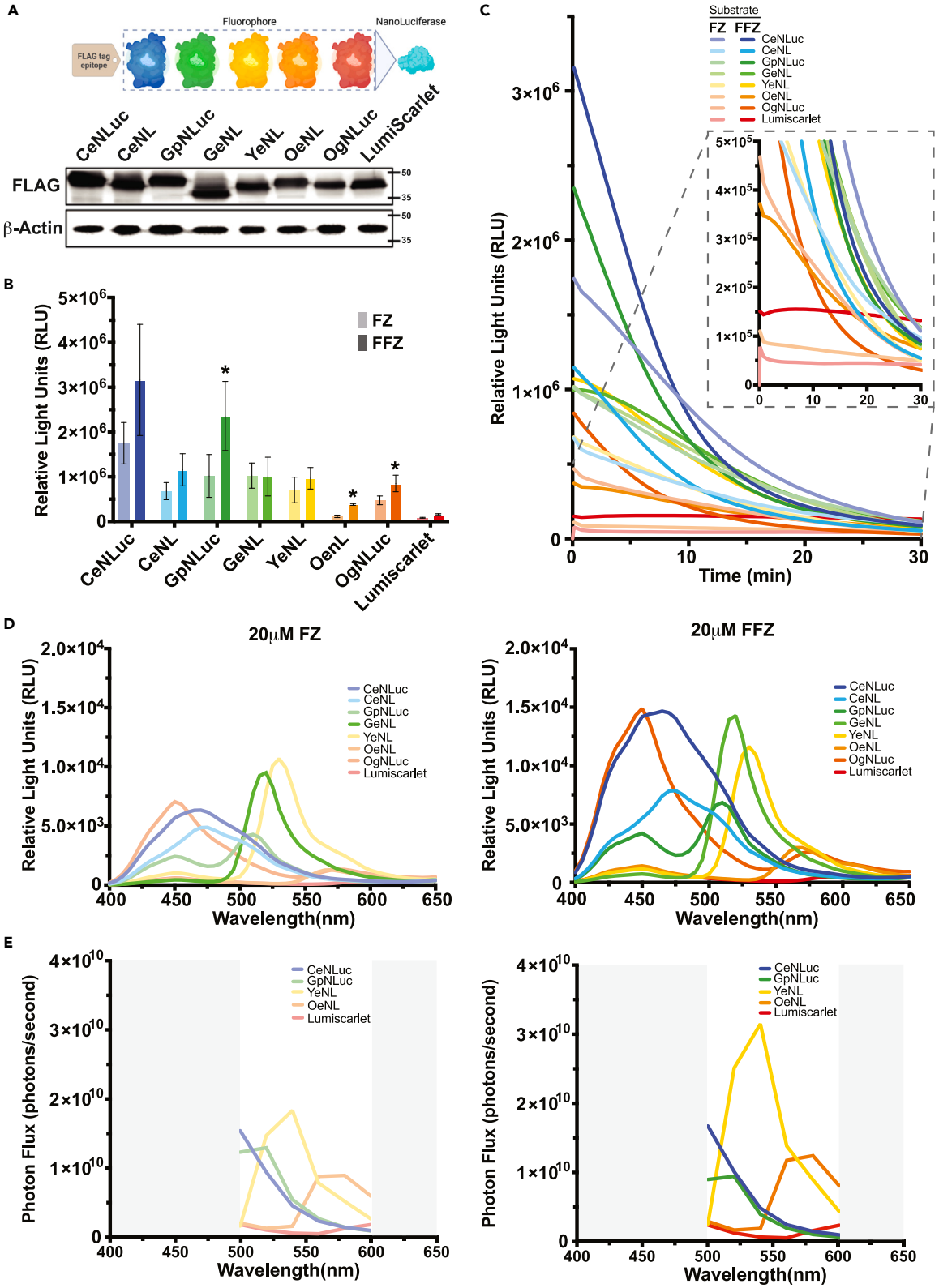
A
Fluorophore
NanoLuciferase
FLAG tag epitope
CeNLuc
CeNL
GpNLuc
GeNL
YeNL
OeNL
OgNLuc
LumiScarlet
FLAG
β-Actin
50
35
B
Relative Light Units (RLU)
FZ
FFZ
C
Substrate
FZ FFZ
Relative Light Units (RLU)
Time (min)
D
20μM FZ
20μM FFZ
Relative Light Units (RLU)
Wavelength(nm)
E
Photon Flux (photons/second)
Wavelength(nm)

Figure 1. Spectral characterization of nanoluciferase-based BRET reporters

(A) Illustration of the FLAG epitope-tagged BRET reporter proteins (*top*) and representative western blot (*bottom*). Data are representative of three independent biological replicates.

(B) Analysis of maximal light output at the peak wavelength produced from stably transduced UM-HMC1 cell lines following administration of 20 μM FFZ versus FZ for each BRET reporter. Error bars show SEM ($n = 3$), $^*P < 0.05$.

(C) Kinetic decay curve parameters for each BRET reporter established following administration of either 20 μM of FZ or FFZ and total light output measurements were collected every 5–8 s over a 30-min imaging session. Data are representative of three independent measurements and reflect mean ± SEM with the inset highlighting curve profiles less than 500,000 RLUs.

(D) Monochromator-based (Cytation5) emission spectra of each BRET reporter following administration of 20 μM FZ (*left*) or FFZ (*right*). Spectra are representative of data from triplicate measurements ($n = 3$).

(E) CCD camera and filter-based approach (IVIS) emission spectra of each BRET reporter following administration of 20 μM FZ (*left*) or FFZ (*right*). Spectra are representative of data from triplicate measurements ($n = 4$).

Next, we used the stable reporter cell lines to seed each of the five 3-color reporter combinations as mixtures with cell reporter color ratios ranging from 100% to 0% relative to one another and examined spectral unmixing performance using 20 μM FZ as the substrate (Figures 2B–2D; Figures S5 and S6). Remarkably, highly efficient spectral unmixing was achieved for a 2-color combination involving GpNLuc and GeNL despite only an 8 nm spectral separation between these two green channel reporters suggesting that spectral separation should not be the only factor used when deciding color combinations (Figure S7). Notably, the GpNLuc reporter consistently produced ~2-fold higher signals with photon emissions of ~1.5×10^9 p/sec/cm^2/sr and peaking at ~509 nm. Moreover, GpNLuc afforded sufficient spectral separation (19 nm) from the 528 nm peak of YeNL and (54 nm) the 563 nm peak of OeNL to achieve the most reliable and robust spectral unmixing of signals (Figure 2B, *bottom*). Despite some combinations involving LumiScarlet offering greater spectral separation parameters, spectral unmixing of these combinations was suboptimal. Consequently, GpNLuc/YeNL/OeNL was selected for further validation *in vivo* due to robust dual-color and triple-color unmixing capabilities.

Application of multispectral imaging for simultaneously monitoring three BRET reporters within tumors

To validate the utility of our GpNLuc/YeNL/OeNL triplex reporter panel for BLI imaging from within tissues of living animals, we established subcutaneous xenografts of the stable cell lines either alone as pure single-color populations or as heterogeneous mixtures and acquired tumor growth and longitudinal BLI data for both substrates on alternating dosing schedules (Figure 3A, *top*; Figure S8). Either FZ or FFZ was administered to animals intraperitoneally and then imaged 5 min after injection to capture radiance (p/sec/cm^2/sr) measurements. Similar to the *in vitro* characterization experiments, each stable reporter cell line was combined into mixtures with ratios ranging from 100% to 0% relative to one another such that some tumors represented 100% green GpNLuc, 67% green GpNLuc and 33% yellow YeNL, 67% green GpNLuc and 33% orange OeNL, 100% yellow YeNL, 67% yellow YeNL and 33% orange OeNL, 67% yellow YeNL and 33% green GpNLuc, 100% orange OeNL, 67% orange OeNL and 33% green GpNLuc, 67% orange OeNL and 33% yellow YeNL, or lastly a triplex mixture of 33% green GpNLuc/33% yellow YeNL/33% orange OeNL. The single-color tumors were established to generate a library that was subsequently used for spectral unmixing to calculate the contribution of each BRET reporter signal (Figure 3A, *bottom*). Multispectral unmixing consistently resolved the contributions of each reporter color for most dual-color combinations as tumors developed over time, although FFZ generally produced >10-fold more bioluminescence and some of the time points revealed substrate-dependent differences at the different reporter percentages evaluated (Figures 3B and 3C). These observations were highlighted on days 30 (FZ) and 31 (FFZ) where a green GpNLuc reporter signal is detected by the unmixing procedure despite the absence of this reporter in the 67% yellow YeNL and

Table 2. Substrate-dependent bioluminescence decay kinetics

	Substrate			
	Furimazine (FZ)		Fluorofurimazine (FFZ)	
BRET reporter	Half-life (min)	R^2	Half-life (min)	R^2
CeNLuc	9.464	0.5945	5.031	0.724
CeNL	10.76	0.6953	5.92	0.751
GpNLuc	11.48	0.3678	5.259	0.8871
GeNL	12.62	0.6778	11.96	0.6235
YeNL	10.16	0.5056	9.09	0.8377
OeNL	0.5496	0.6592	0.2111	0.9936
OgNLuc	10.77	0.7994	25.64	0.8446
LumiScarlet	307.7	0.7968	1.412	0.9081

min, minutes; R^2, coefficient of determination for linear regression model.

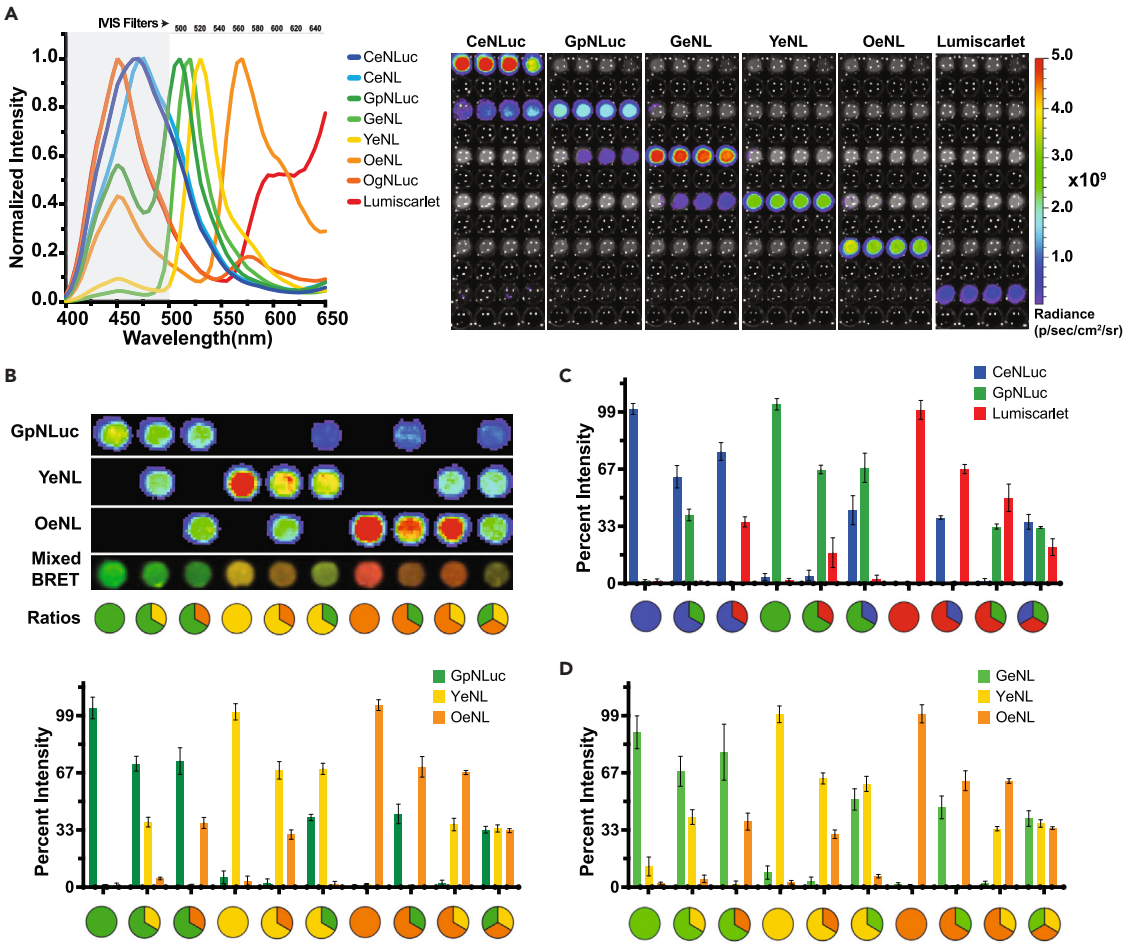

Figure 2. Optimization of triple-color BRET reporter combinations and spectral unmixing

(A) *Left*, comparison of IVIS Spectrum emission filters relative to the normalized emission spectra peaks of each reporter. The grayed box indicates the area of the reporter emission spectrum that the IVIS is unable to capture based on the eight available emission filters spanning 500–640 nm. *Right*, representative unmixed bioluminescent images of stable reporter cell lines seeded in replicates (n = 4) at one ratio (100% unmixed population).

(B) *Top*, application of spectral unmixing to mixed or unmixed populations UM-HMC1 stable cell lines expressing GpNLuc, YeNL, or OeNL BRET reporters at the various proportions of 10,000 cells/well indicated (100%, 67%, and 33%). The plate was imaged following substrate administration and photon output measured using an IVIS system. Spectral unmixing was performed by building a library specific to a pure (i.e., 100%) BRET reporter BLI measurement and then applied to the mixed BRET reporter conditions to generate the composite image presented in the fourth row. The ratio of each reporter cell population is represented by a color-coded pie chart at the bottom of each column. *Bottom*, quantification of bioluminescent signals following FFZ administration (photon flux) and the different percentages of each BRET reporter quantified in relation to the expected proportions indicated (ranging from 100% to 0%). The unmixed bioluminescent signals were normalized to the 100% BRET ratio conditions (n = 3).

(C and D) Spectral unmixing quantification of CeNLuc, GpNLuc, or LumiScarlet (C), versus GeNL, YeNL, or OeNL (D) reporter combinations following FFZ administration (photon flux). Percentages of each BRET reporter quantified in relation to the expected proportions indicated by the corresponding pie charts (ranging from 100% to 0%). The unmixed bioluminescent signals were normalized to the 100% BRET ratio conditions (n = 3).

33% orange OeNL condition and the 67% yellow YeNL and 33% green GpNLuc condition (Figures 3D and 3E). Notably, the ability to successfully unmix multiple BRET reporter probes from the same tumor site *in vivo* composed of 33% of each stable three-color reporter cell line can be achieved *in vivo* with single-substrate administration (Figures S9–S12). For comparison to BLI analysis, tumors were resected and dissociated at endpoint, and flow cytometry was performed to measure the relative contribution of each expected color percentage (Figure S13). Despite some discordance between methodologies, applying spectral compensation to the flow cytometric data confirmed that the standard deviation of signal averages largely overlap for the reporter percentages calculated from flow cytometry and BLI.

DISCUSSION

Methodologies employing BRET-based tools have emerged as highly desirable approaches for monitoring a variety of processes ranging from cell signaling to protein-protein interactions, among others.[3,25–30] For example, a multitude of engineered BRET-based optical reporters

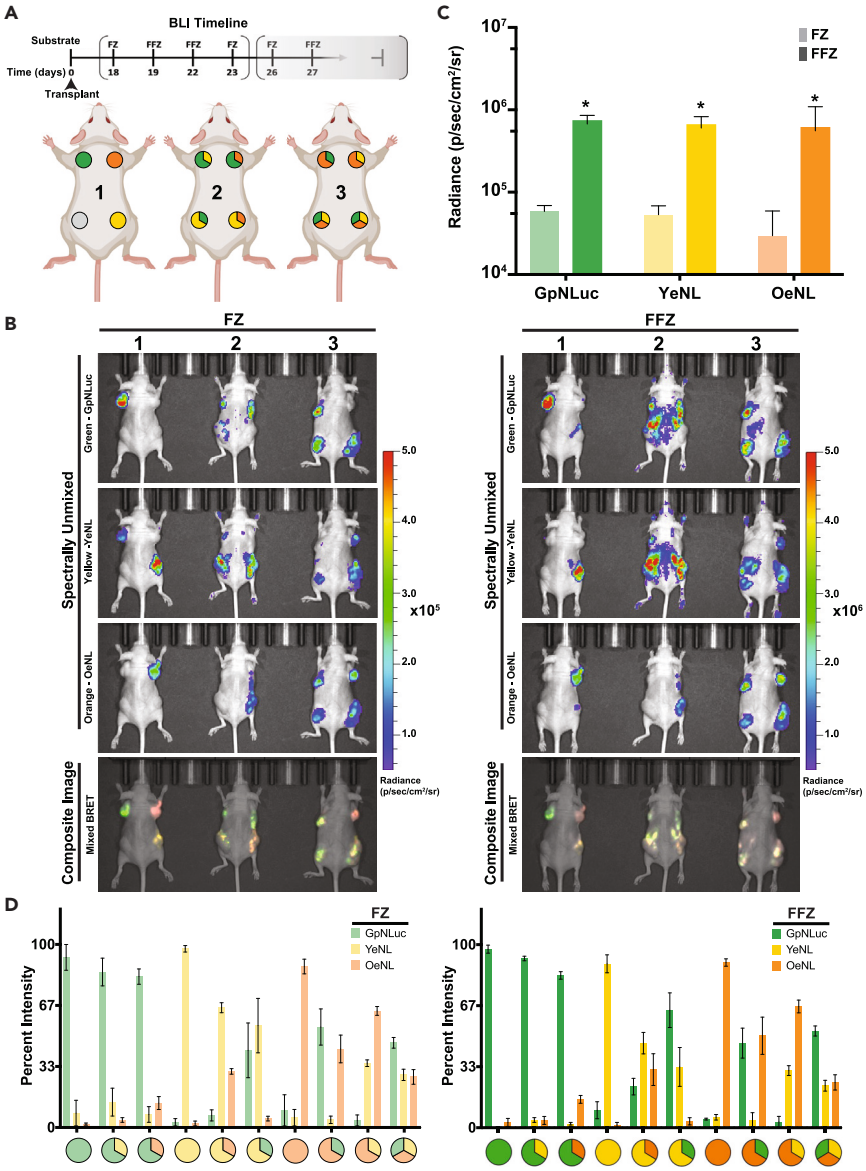

Figure 3. Demonstration of single-substrate multispectral imaging of three independent tumor cell populations *in vivo*

(A) Schematic of the BLI session timeline with corresponding substrate that was administered (*top*) and the *in vivo* experimental setup including the location and proportions of each population of transplanted stable tumor cell line(s) as indicated (100%, 67%, and 33%) by inset pie charts (*bottom*).

(B) Spectral unmixing of either mixed or unmixed tumor xenografts expressing GpNLuc, YeNL, or OeNL BRET reporters at the various proportions indicated following either FZ (*left*) or FFZ (*right*) administration. Animals were imaged following substrate administration and photon output measured using an IVIS system. Spectral unmixing was performed by building a library specific to a pure (i.e., 100%) BRET reporter BLI measurement and then applied to the mixed BRET reporter conditions to generate the composite image presented in the fourth row.

(C) Comparison of bioluminescence emission (radiance; CCD camera) for FZ versus FFZ produced by tumor xenografts composed of 100% of each respective BRET reporter ($n = 4$), $^*P < 0.05$.

(D) Quantification of spectrally unmixed bioluminescent signals following either FZ (*left*) or FFZ (*right*) administration (photon flux). Percentages of each BRET reporter quantified in relation to the expected proportions indicated by the corresponding pie charts (ranging from 100% to 0%). The ratio of each reporter cell population is represented by a color-coded pie chart at the bottom of each group. The unmixed bioluminescent signals were normalized to the 100% BRET ratio conditions ($n = 4$).

employing NanoLuc have been developed and some involve the utilization of NanoLuc variants with novel substrate analogs.[15,31–33] Early examples include LumiFluor reporters, which were specifically engineered to enhance spectral emission (e.g., increased quantum yield) and *in vivo* tissue penetration to increase signal detection and improve BLI data acquisition in tumor models.[15] These marine luciferase-based

reporters are particularly attractive for pre-clinical oncology studies since they are ATP independent compared to their firefly counterparts.[3] Specifically, there is a growing appreciation for the impact of ATP-dependent firefly luciferases on cells since it is estimated that 2.5 ATP molecules are consumed per catalytic reaction cycle to produce bioluminescence.[34] This can place a significant metabolic burden on cells when considering that luciferases are frequently expressed at the micromolar level within cells and that most pre-clinical oncology studies span several weeks to months.[35,36] Notably, the dual BLI studies performed to date have employed at least one ATP-dependent firefly or click beetle luciferase.[22,23,37–42] In addition to engineering these luminescent-fluorescent biological light sources, significant progress has also been made in engineering orthogonal substrates for several luciferases, which has created an opportunity to envision a variety of multiplexed imaging strategies.[2,18,20,21,43] However, while orthologous substrates enable the specific detection and temporary resolution of signals emanating from distinct cell types both *in vitro* and *in vivo*, it necessitates a multi-dosing regimen wherein administration of the first substrate illuminates one cell type/population and this must be followed by a "washout" or active quenching period (few hours to days) before which a subsequent substrate can be administered and a different cell type/population can be imaged. Consequently, this approach is technically challenging *in vivo*, resource intensive, and places animal subjects in undue stress, which can influence study outcomes. This is especially important for longitudinal oncology studies where animal stress can affect tumor vascularization, drug bio-distribution/degradation, and other aspects of tumor behavior that can influence response to therapeutic interventions. Thus, *in vivo* BLI strategies that employ single-substrate administration, yet offer the ability to resolve multiple independent parameters with minimal impact to test subjects, are urgently needed.

Here, we report on a novel triple-color BLI assay paradigm with the ability to unmix three distinct tumor cell populations using a single substrate, which afforded high sensitivity and minimal animal discomfort throughout the course of the 5-week study. Simultaneous two-color *in vivo* BLI is readily achieved and now routinely applied using single specialized substrates (e.g., diphenylterazine, NH_2-NpLH2, and AkaLumine); however, these strategies are technically challenging to implement and often depend on substrates that are not commercially available, and these substrates lack standardized synthesis and quality control. Thus, there is an increasing demand for establishing rigorous methodologies to successfully achieve temporal and spectral resolution of more than two colors using readily available reagents. This potential for multispectral BLI is evident by our ability to resolve two green BRET reporters (i.e., GeNL and GpNLuc) via spectral unmixing and without having to rely on multiple or orthogonal substrates. Consequently, we tested the ability to perform triple-color *in vivo* BLI using well-established and routinely used BRET reporters coupled with commercially available, affordable, and widespread substrates and imaging modalities that can be deployed in most labs at no added cost.

The feasibility and brightness of our three-color BLI system was established by first generating a panel of FLAG epitope-tagged versions for nearly all available NanoLuc-based BRET reporters within a common lentiviral mammalian expression vector. These reporters were then rigorously evaluated both *in vitro* and *in vivo* to assess their bioluminescent performance during catalysis of two coelenterazine-based substrate analogs (i.e., FZ and FFZ). Confirming previous reports, we found that FFZ leads to ~10-fold higher peak signal output compared to FZ, albeit at the cost of a more stable half-life afforded by FZ.[22,44] The CeNLuc and CeNL reporters were initially considered for multispectral BLI since these reporters produce intense signals and display a broad spectral profile that carries into the 500 nm range where most IVIS systems have emission filters, although a band-pass emission filter at 480 nm would be ideal for combinations involving these reporters given their modest spectral separation from GpNLuc (34 nm) and GeNL (42 nm). In the present study, we analyzed six unique three-color BRET reporter combinations and tested each with both FZ and FFZ substrates, which identified GpNLuc/YeNL/OeNL as an optimal combination. This combination is likely optimal because, of all the various reporter combinations examined, each individual reporter exhibits the most comparable light outputs. This suggests that, when simultaneously unmixing multiple reporters, it is important to consider not only spectrally separated reporters but also those that are closely matched in their peak light outputs. By having similar outputs, one avoids overestimation of the brighter reporters compared to dimmer reporters (e.g., GeNL/YeNL/OgNLuc relative to GpNLuc/YeNL/OeNL). Thus, enhancing the peak light output of orange-red reporters will likely help further improve triple-color unmixing, which, when combined with addition of blue-shifted filter sets, may pave the way for simultaneous single-substrate unmixing of four to five colors within an *in vivo* setting.

Collectively, not only does the present work show it is feasible to successfully unmix GpNLuc/YeNL/OeNL, but that this approach also allows for robust and highly reproducible *in vivo* BRET imaging using a single substrate for the detection of three distinct tumor cell populations. For example, this study lays to groundwork for future investigations that seek to longitudinally track tumor heterogeneity using *in vivo* BLI. However, the application of this three-color BRET system requires careful consideration to the predicted or known relative abundance of the target cell types under investigation to ensure reliable spectral unmixing. Specifically, our analyses reveal that the signal produced by green BRET reporters can be overestimated during the unmixing process, while the signal produced by orange BRET reporters can be underestimated, likely due to the relative signal bleed-through between spectrally similar reporters and adjacent band-pass emission filters, which are designed with a 20 nm spectral resolution. However, this experimental artifact can be easily overcome by ensuring that the population found in the largest proportion (e.g., tumor cell) is labeled in orange and that the other rarer cell populations of interest (e.g., cancer stem cells/tumor-initiating cells versus tumor propagating cells, chimeric antigen receptor [CAR]-T cells, CAR-natural killer cells, or antibody-drug conjugate therapeutic[16]) are labeled with the green or yellow BRET reporters. Collectively, this work has validated the feasibility of performing triplex BLI for visualizing the location, evolution, and other aspects of tumor biology, which will greatly facilitate both basic and translational investigations.

Limitations of the study

While multispectral unmixing resolved the contributions of each reporter color over time as tumors developed, some of the time points revealed substrate-dependent differences that may be due to differences in tumor volumes, O_2 availability (i.e., angiogenesis/hypoxia),

and photon scattering and/or penetration (Figure S9). Moreover, we and others previously showed that the route of substrate delivery can influence *in vivo* BLI, but the present study did not assess if this parameter has any impact on the three-color BLI unmixing. This study also did not compare other more recently developed coelenterazine analogs such as hydrofurimazine,[22] cephalofurimazine,[45] and quinolinylterazine[32] and did not account for populations of cells with differing growth rates. Lastly, the potential applicability of multispectral *in vivo* BLI is deeply tied to the spectral resolution of the imaging modalities used to reliably unmix these signals. Despite CeNLuc's bright signal, it cannot be deployed *in vivo* not only due to its poorer tissue penetration and higher scattering compared to a red-shifted reporters but also because most commercially available, off-the-shelf imaging modalities such as the IVIS only detect light >500 nm. This instrument limitation entirely excludes peak light emission profiles of blue BRET reporters (~475 nm). Adding additional light filters to these imaging instruments may further unlock their full potential and perhaps someday enable multispectral BLI of four to five colors *in vivo*.

STAR★METHODS

Detailed methods are provided in the online version of this paper and include the following:

- KEY RESOURCES TABLE
- RESOURCE AVAILABILITY
  - Lead contact
  - Materials availability
  - Data and code availability
- EXPERIMENTAL MODEL DETAILS
  - Mouse models
  - Subcutaneous tumor xenograft
  - *In vivo* imaging
- METHOD DETAILS
  - Plasmid construction and stable cell line generation
  - Western blotting
  - Spectral emission profiles
  - Kinetic decay curves
  - *In vitro* cell proliferation
  - *In vitro* cell imaging
  - Flow cytometry
- QUANTIFICATION AND STATISTICAL ANALYSES

SUPPLEMENTAL INFORMATION

Supplemental information can be found online at https://doi.org/10.1016/j.isci.2024.110655.

ACKNOWLEDGMENTS

The authors thank Charlene Santos and Hong Yuan of the UNC-Chapel Hill Animal Studies Core (ASC) and Small Animal Imaging Facility, respectively. We thank Jodie Kroeger of the H. Lee Moffitt Cancer Center & Research Institute Flow Cytometry Core for expert technical assistance and members of the Amelio Lab for helpful discussions, suggestions, and/or scientific review of this article. This work was supported in part by an Allen Distinguished Investigator Award, a Paul G. Allen Frontiers Group advised grant of the Paul G. Allen Family Foundation (to J.A.P.), and NIH/NIDCR R01DE030123 and funding support from the State of Florida (to A.L.A.). The UNC Lineberger and Moffitt Shared Resources Cores are supported in part by 5P30CA016080-42 and P30-CA076292 NCI Support Grants to each Comprehensive Cancer Center, respectively.

AUTHOR CONTRIBUTIONS

Conception and design, B.L., K.P.-S., and A.L.A.; development of methodology, B.L., K.P.-S., J.J.P., and A.L.A.; acquisition of data (provided reagents, provided facilities, etc.), B.L., K.P.-S., J.J.P., S.S., and J.R.W.; interpretation of data (e.g., statistical analysis, biostatistics, and computational analysis), B.L., K.P.-S., J.J.P., and A.L.A.; writing of the manuscript, B.L., K.P.-S., J.J.P., and A.L.A.; review and revision of the manuscript, B.L., K.P.-S., J.J.P., S.S., J.R.W., T.A.K., C.K.B., J.A.P., and A.L.A.; administrative, technical, or material support (i.e., reporting or organizing data and constructing databases), J.J.P., S.S., J.R.W., and C.K.B.; study supervision, K.P.-S. and A.L.A.; acquisition of funding, A.L.A.

DECLARATION OF INTERESTS

T.A.K. is an employee of Promega Corporation. J.R.W. and T.A.K. are inventors on a patent describing furimazine and furimazine derivatives. A.L.A. is a Global Advisory Board member and paid consultant for LG Chem Life Sciences Innovation Center.

DECLARATION OF GENERATIVE AI AND AI-ASSISTED TECHNOLOGIES IN THE WRITING PROCESS

During the preparation of this work, the authors used ChatGPT 4.0 in order to shorten the Summary section from 215 words to 147 words. After using ChatGPT 4.0, the authors reviewed and edited the content as needed and take full responsibility for the content of the publication.

Received: February 12, 2024
Revised: April 30, 2024
Accepted: July 31, 2024
Published: August 8, 2024

REFERENCES

1. Weissleder, R., and Pittet, M.J. (2008). Imaging in the era of molecular oncology. Nature *452*, 580–589. https://doi.org/10.1038/nature06917.
2. Williams, S.J., and Prescher, J.A. (2019). Building Biological Flashlights: Orthogonal Luciferases and Luciferins for *in Vivo* Imaging. Acc. Chem. Res. *52*, 3039–3050. https://doi.org/10.1021/acs.accounts.9b00391.
3. Zambito, G., Chawda, C., and Mezzanotte, L. (2021). Emerging tools for bioluminescence imaging. Curr. Opin. Chem. Biol. *63*, 86–94. https://doi.org/10.1016/j.cbpa.2021.02.005.
4. Xu, T., Close, D., Handagama, W., Marr, E., Sayler, G., and Ripp, S. (2016). The Expanding Toolbox of In Vivo Bioluminescent Imaging. Front. Oncol. *6*, 150. https://doi.org/10.3389/fonc.2016.00150.
5. Delroisse, J., Duchatelet, L., Flammang, P., and Mallefet, J. (2021). Leaving the Dark Side? Insights Into the Evolution of Luciferases. Front. Mar. Sci. *8*, 673620. https://doi.org/10.3389/fmars.2021.673620.
6. Hanahan, D., and Weinberg, R.A. (2011). Hallmarks of cancer: the next generation. Cell *144*, 646–674. https://doi.org/10.1016/j.cell.2011.02.013.
7. Condeelis, J., and Weissleder, R. (2010). In vivo imaging in cancer. Cold Spring Harb. Perspect. Biol. *2*, a003848. https://doi.org/10.1101/cshperspect.a003848.
8. Ellenbroek, S.I.J., and van Rheenen, J. (2014). Imaging hallmarks of cancer in living mice. Nat. Rev. Cancer *14*, 406–418. https://doi.org/10.1038/nrc3742.
9. Welsh, D.K., and Noguchi, T. (2012). Cellular bioluminescence imaging. Cold Spring Harbor Protoc. *2012*, pdb-top070607. https://doi.org/10.1101/pdb.top070607.
10. Hajaj, E., Sciacovelli, M., Frezza, C., and Erez, A. (2021). The context-specific roles of urea cycle enzymes in tumorigenesis. Mol. Cell *81*, 3749–3759. https://doi.org/10.1016/j.molcel.2021.08.005.
11. Sloas, D.C., Tran, J.C., Marzilli, A.M., and Ngo, J.T. (2023). Tension-tuned receptors for synthetic mechanotransduction and intercellular force detection. Nat. Biotechnol. *41*, 1287–1295. https://doi.org/10.1038/s41587-022-01638-y.
12. Hall, M.P., Unch, J., Binkowski, B.F., Valley, M.P., Butler, B.L., Wood, M.G., Otto, P., Zimmerman, K., Vidugiris, G., Machleidt, T., et al. (2012). Engineered luciferase reporter from a deep sea shrimp utilizing a novel imidazopyrazinone substrate. ACS Chem. Biol. *7*, 1848–1857. https://doi.org/10.1021/cb3002478.
13. Law, G.H.E., Gandelman, O.A., Tisi, L.C., Lowe, C.R., and Murray, J.A.H. (2006). Mutagenesis of solvent-exposed amino acids in Photinus pyralis luciferase improves thermostability and pH-tolerance. Biochem. J. *397*, 305–312. https://doi.org/10.1042/BJ20051847.
14. Viviani, V.R. (2002). The origin, diversity, and structure function relationships of insect luciferases. Cell. Mol. Life Sci. *59*, 1833–1850. https://doi.org/10.1007/pl00012509.
15. Schaub, F.X., Reza, M.S., Flaveny, C.A., Li, W., Musicant, A.M., Hoxha, S., Guo, M., Cleveland, J.L., and Amelio, A.L. (2015). Fluorophore-NanoLuc BRET Reporters Enable Sensitive In Vivo Optical Imaging and Flow Cytometry for Monitoring Tumorigenesis. Cancer Res. *75*, 5023–5033. https://doi.org/10.1158/0008-5472.CAN-14-3538.
16. Tang, Y., Parag-Sharma, K., Amelio, A.L., and Cao, Y. (2019). A Bioluminescence Resonance Energy Transfer-Based Approach for Determining Antibody-Receptor Occupancy In Vivo. iScience *15*, 439–451. https://doi.org/10.1016/j.isci.2019.05.003.
17. Suzuki, K., Kimura, T., Shinoda, H., Bai, G., Daniels, M.J., Arai, Y., Nakano, M., and Nagai, T. (2016). Five colour variants of bright luminescent protein for real-time multicolour bioimaging. Nat. Commun. *7*, 13718. https://doi.org/10.1038/ncomms13718.
18. Yeh, H.W., Xiong, Y., Wu, T., Chen, M., Ji, A., Li, X., and Ai, H.W. (2019). ATP-Independent Bioluminescent Reporter Variants To Improve in Vivo Imaging. ACS Chem. Biol. *14*, 959–965. https://doi.org/10.1021/acschembio.9b00150.
19. Gibbons, A.E., Luker, K.E., and Luker, G.D. (2018). Dual Reporter Bioluminescence Imaging with NanoLuc and Firefly Luciferase. Methods Mol. Biol. *1790*, 41–50. https://doi.org/10.1007/978-1-4939-7860-1_4.
20. Brennan, C.K., Yao, Z., Ionkina, A.A., Rathbun, C.M., Sathishkumar, B., and Prescher, J.A. (2022). Multiplexed bioluminescence imaging with a substrate unmixing platform. Cell Chem. Biol. *29*, 1649–1660.e4. https://doi.org/10.1016/j.chembiol.2022.10.004.
21. Brennan, C.K., Ornelas, M.Y., Yao, Z.W., and Prescher, J.A. (2021). Multicomponent Bioluminescence Imaging with Naphthylamino Luciferins. Chembiochem *22*, 2650–2654. https://doi.org/10.1002/cbic.202100202.
22. Su, Y., Walker, J.R., Park, Y., Smith, T.P., Liu, L.X., Hall, M.P., Labanieh, L., Hurst, R., Wang, D.C., Encell, L.P., et al. (2020). Novel NanoLuc substrates enable bright two-population bioluminescence imaging in animals. Nat. Methods *17*, 852–860. https://doi.org/10.1038/s41592-020-0889-6.
23. Stowe, C.L., Burley, T.A., Allan, H., Vinci, M., Kramer-Marek, G., Ciobota, D.M., Parkinson, G.N., Southworth, T.L., Agliardi, G., Hotblack, A., et al. (2019). Near-infrared dual bioluminescence imaging in mouse models of cancer using infraluciferin. Elife *8*, e45801. https://doi.org/10.7554/eLife.45801.
24. Taylor, A., Sharkey, J., Plagge, A., Wilm, B., and Murray, P. (2018). Multicolour In Vivo Bioluminescence Imaging Using a NanoLuc-Based BRET Reporter in Combination with Firefly Luciferase. Contrast Media Mol. Imaging *2018*, 2514796. https://doi.org/10.1155/2018/2514796.
25. Weihs, F., Wang, J., Pfleger, K.D.G., and Dacres, H. (2020). Experimental determination of the bioluminescence resonance energy transfer (BRET) Forster distances of NanoBRET and red-shifted BRET pairs. Anal. Chim. Acta X *6*, 100059. https://doi.org/10.1016/j.acax.2020.100059.
26. Alves, J., Schwinn, M., Machleidt, T., Goueli, S.A., Cali, J.J., and Zegzouti, H. (2024). Monitoring phosphorylation and acetylation of CRISPR-mediated HiBiT-tagged endogenous proteins. Sci. Rep. *14*, 2138. https://doi.org/10.1038/s41598-024-51887-x.
27. Kobayashi, H., Picard, L.P., Schönegge, A.M., and Bouvier, M. (2019). Bioluminescence resonance energy transfer-based imaging of protein-protein interactions in living cells. Nat. Protoc. *14*, 1084–1107. https://doi.org/10.1038/s41596-019-0129-7.
28. De, A. (2011). The new era of bioluminescence resonance energy transfer technology. Curr. Pharm. Biotechnol. *12*, 558–568. https://doi.org/10.2174/138920111795163922.
29. Love, A.C., and Prescher, J.A. (2020). Seeing (and Using) the Light: Recent Developments in Bioluminescence Technology. Cell Chem. Biol. *27*, 904–920. https://doi.org/10.1016/j.chembiol.2020.07.022.
30. Yao, Z., Zhang, B.S., and Prescher, J.A. (2018). Advances in bioluminescence imaging: new probes from old recipes. Curr. Opin. Chem. Biol. *45*, 148–156.
31. Liu, S., Su, Y., Lin, M.Z., and Ronald, J.A. (2021). Brightening up Biology: Advances in Luciferase Systems for *in Vivo* Imaging. ACS Chem. Biol. *16*, 2707–2718. https://doi.org/10.1021/acschembio.1c00549.
32. Xiong, Y., Zhang, Y., Li, Z., Reza, M.S., Li, X., Tian, X., and Ai, H.W. (2022). Engineered Amber-Emitting Nano Luciferase and Its Use for Immunobioluminescence Imaging *In Vivo*. J. Am. Chem. Soc. *144*, 14101–14111. https://doi.org/10.1021/jacs.2c02320.
33. Shakhmin, A., Hall, M.P., Machleidt, T., Walker, J.R., Wood, K.V., and Kirkland, T.A. (2017). Coelenterazine analogues emit red-shifted bioluminescence with NanoLuc. Org. Biomol. Chem. *15*, 8559–8567. https://doi.org/10.1039/c7ob01985h.
34. Yeh, H.W., Wu, T., Chen, M., and Ai, H.W. (2019). Identification of Factors Complicating Bioluminescence Imaging. Biochemistry *58*,

1689–1697. https://doi.org/10.1021/acs.biochem.8b01303.

35. Zhou, Y., Tozzi, F., Chen, J., Fan, F., Xia, L., Wang, J., Gao, G., Zhang, A., Xia, X., Brasher, H., et al. (2012). Intracellular ATP levels are a pivotal determinant of chemoresistance in colon cancer cells. Cancer Res. *72*, 304–314. https://doi.org/10.1158/0008-5472.CAN-11-1674.
36. Wang, T., Ma, F., and Qian, H.L. (2021). Defueling the cancer: ATP synthase as an emerging target in cancer therapy. Mol. Ther. Oncolytics *23*, 82–95. https://doi.org/10.1016/j.omto.2021.08.015.
37. Zambito, G., Mishra, G., Schliehe, C., and Mezzanotte, L. (2022). Near-Infrared Bioluminescence Imaging of Macrophage Sensors for Cancer Detection *In Vivo*. Front. Bioeng. Biotechnol. *10*, 867164. https://doi.org/10.3389/fbioe.2022.867164.
38. Zambito, G., and Mezzanotte, L. (2021). Near-infrared bioluminescence imaging of two cell populations in living mice. STAR Protoc. *2*, 100662. https://doi.org/10.1016/j.xpro.2021.100662.
39. Zambito, G., Hall, M.P., Wood, M.G., Gaspar, N., Ridwan, Y., Stellari, F.F., Shi, C., Kirkland, T.A., Encell, L.P., Löwik, C., and Mezzanotte, L. (2021). Red-shifted click beetle luciferase mutant expands the multicolor bioluminescent palette for deep tissue imaging. iScience *24*, 101986. https://doi.org/10.1016/j.isci.2020.101986.
40. Zambito, G., Gaspar, N., Ridwan, Y., Hall, M.P., Shi, C., Kirkland, T.A., Encell, L.P., Löwik, C., and Mezzanotte, L. (2020). Evaluating Brightness and Spectral Properties of Click Beetle and Firefly Luciferases Using Luciferin Analogues: Identification of Preferred Pairings of Luciferase and Substrate for In Vivo Bioluminescence Imaging. Mol. Imaging Biol. *22*, 1523–1531. https://doi.org/10.1007/s11307-020-01523-7.
41. Hall, M.P., Woodroofe, C.C., Wood, M.G., Que, I., van't Root, M., Ridwan, Y., Shi, C., Kirkland, T.A., Encell, L.P., Wood, K.V., et al. (2018). Click beetle luciferase mutant and near infrared naphthyl-luciferins for improved bioluminescence imaging. Nat. Comm. *9*, 132. https://doi.org/10.1038/s41467-017-02542-9.
42. Branchini, B.R., Ablamsky, D.M., Davis, A.L., Southworth, T.L., Butler, B., Fan, F., Jathoul, A.P., and Pule, M.A. (2010). Red-emitting luciferases for bioluminescence reporter and imaging applications. Anal. Biochem. *396*, 290–297. https://doi.org/10.1016/j.ab.2009.09.009.
43. Rathbun, C.M., Ionkina, A.A., Yao, Z., Jones, K.A., Porterfield, W.B., and Prescher, J.A. (2021). Rapid Multicomponent Bioluminescence Imaging *via* Substrate Unmixing. ACS Chem. Biol. *16*, 682–690. https://doi.org/10.1021/acschembio.0c00959.
44. Gaspar, N., Walker, J.R., Zambito, G., Marella-Panth, K., Lowik, C., Kirkland, T.A., and Mezzanotte, L. (2021). Evaluation of NanoLuc substrates for bioluminescence imaging of transferred cells in mice. J. Photochem. Photobiol., B *216*, 112128. https://doi.org/10.1016/j.jphotobiol.2021.112128.
45. Su, Y., Walker, J.R., Hall, M.P., Klein, M.A., Wu, X., Encell, L.P., Casey, K.M., Liu, L.X., Hong, G., Lin, M.Z., and Kirkland, T.A. (2023). An optimized bioluminescent substrate for non-invasive imaging in the brain. Nat. Chem. Biol. *19*, 731–739. https://doi.org/10.1038/s41589-023-01265-x.
46. Tomayko, M.M., and Reynolds, C.P. (1989). Determination of subcutaneous tumor size in athymic (nude) mice. Cancer Chemother. Pharmacol. *24*, 148–154.
47. Musicant, A.M., Parag-Sharma, K., Gong, W., Sengupta, M., Chatterjee, A., Henry, E.C., Tsai, Y.H., Hayward, M.C., Sheth, S., Betancourt, R., et al. (2021). CRTC1/MAML2 directs a PGC-1alpha-IGF-1 circuit that confers vulnerability to PPARgamma inhibition. Cell Rep. *34*, 108768. https://doi.org/10.1016/j.celrep.2021.108768.

STAR★METHODS

KEY RESOURCES TABLE

REAGENT or RESOURCE	SOURCE	IDENTIFIER
Antibodies		
Mouse monoclonal anti-FLAG HRP conjugated antibody	Millipore-Sigma	Cat# A8592; RRID: AB_439702
Mouse monoclonal anti- β-actin antibody	Millipore-Sigma	Cat# A1978; RRID: AB_476692
Rabbit anti-Mouse IgG (H + L) Secondary Antibody, HRP	Thermo Fisher Scientific	Cat# 31450; RRID: AB_228427
Bacterial and virus strains		
Escherichia coli: Chemically Competent Stbl3	Thermo Fisher Scientific	Cat#C737303
Chemicals, peptides, and recombinant proteins		
Furimazine (FZ)	Promega	Cat# N113B
Fluorofurimazine (FFZ)	Promega	N/A
Y27632 (ROCK inhibitor)	Selleckchem	Cat# S1049
Critical commercial assays		
BCA assay	Thermo Fisher Scientific	Cat# 23225
Experimental models: Cell lines		
UM-HMC-1	Laboratory of Jacques E. Nör (University of Michigan, Ann Arbor, MI)	RRID: CVCL_Y473
Experimental models: Organisms/strains		
Mouse: Nu/Nu	The Jackson Laboratory	RRID: IMSR_JAX:002019
Oligonucleotides		
Primers for pLenti cloning, see Table S2	This paper	N/A
Recombinant DNA		
pLenti-CMV-MCS-SV40-Puro	This paper	N/A
pLenti_CMV:Flag-CeNLuc	This paper	Addgene Plasmid #208838
pLenti_CMV:Flag-CeNL	This paper	Addgene Plasmid #208839
pLenti_CMV:Flag-GpNLuc	This paper	Addgene Plasmid #208840
pLenti_CMV:Flag-GeNL	This paper	Addgene Plasmid #208841
pLenti_CMV:Flag-YeNL	This paper	Addgene Plasmid #208849
pLenti_CMV:Flag-OeNL	This paper	Addgene Plasmid #208850
pLenti_CMV:Flag-OgNLuc	This paper	Addgene Plasmid #208851
pLenti_CMV:Flag-Antares	This paper	Addgene Plasmid #208852
pLenti_CMV:Flag-Lumiscarlet	This paper	Addgene Plasmid #208854
pLenti_CMV:Flag-KaNLuc	This paper	Addgene Plasmid #208855
pLenti_CMV:Flag-dKeNLuc	This paper	Addgene Plasmid #208856
Software and algorithms		
GraphPad Prism (version 9)	GraphPad Software, Inc.	https://www.graphpad.com
FlowJo v10.8 software	BD Life Sciences	https://www.flowjo.com/
IVIS software: Living Image (version 4.5.4)	PerkinElmer	https://resources.perkinelmer.com/corporate/content/lst_software_downloads/living_image_4.5_installation_licensing_guide.pdf

RESOURCE AVAILABILITY

Lead contact

Further information and requests for resources and reagents should be directed to and will be fulfilled by the Lead Contact, Antonio L. Amelio (antonio.amelio@moffitt.org).

Materials availability

The plasmids generated in this study are outlined in the key resources table and have been deposited with Addgene. Cell lines generated in this study are available from the lead contact upon request via a material transfer agreement (MTA).

Data and code availability

- Data Availability: The raw BLI data analyzed for this study were generated using the IVIS Spectrum at the UNC Small Animal Imaging Facility. Derived data supporting the findings of this study are available from the lead contact upon request.
- Code availability: All computer code employed are commercially available. No custom computer code were generated or used for the analyses performed in this study.
- Additional information: Any additional information required to analyze the data reported in this work paper is available from the lead contact upon request.

EXPERIMENTAL MODEL DETAILS

Mouse models

All animal studies were reviewed and approved by The University of North Carolina at Chapel Hill Institutional Animal Care and Use Committee under IACUC protocol 17–202. Male and Female 6–8 week old athymic nude mice (Nu/Nu) were obtained from the Animal Studies Core at the University of North Carolina at Chapel Hill and housed in facilities run by the Division of Comparative Medicine at the University of North Carolina (Chapel Hill, NC, USA).

Subcutaneous tumor xenograft

The UM-HMC-1 cell cultures (RRID: CVCL_Y473) expressing GpNLuc, YeNL, and OeNL were kept under 0.5 μg/mL puromycin selection until the culture reached 80–90% confluency. These were then passaged, through trypsin dissociation (TrypLE Express, Thermo Fisher cat# 12604039) and aliquoted into the appropriate ratios with a total of 3×10^5 cells to be injected per tumor site. Seven unique reporter combinations were formulated along with three control tumors containing a single reporter and one tumor containing no reporters. These mixtures were then pelleted at 600 × g for 5 min and resuspended in ice-cold HBSS (Gibco, cat# 14175-095) and kept on ice until the time of transplant where each suspension of cells and HBSS were thoroughly mixed with an equal volume of ice-cold Cultrex Basement Membrane Extract (R&D Systems, cat# 343200501P) 100 μL of this mixture was injected subcutaneously into one of four dorsal regions of the athymic nude mouse (RRID: MGI:5649750). Each of the twelve mice received a total of four implants as previously described.[15] Tumor volume was obtained with external calipers measurements of the length and width of the tumor immediately after each imaging session. The calculation of tumor volume employed a modified ellipsoidal formula: Tumor volume = 1/2(length × width^2).[46]

In vivo imaging

Imaging sessions began at day 18 and 19 post-transplant and continued every 3rd and 4th day, alternating between which substrate was administered on the first of two days, as seen in Figure 3A. Twelve mice were split into three groups of four. Each group was anesthetized, following appropriate IACUC guidelines in isoflurane anesthesia, and imaged 5 min after intraperitoneal administration of 25nmol FZ or 125nmol FFZ reconstituted in 100 μL of room temperature DPBS (Corning, ref# 21-031-CV). Images were acquired using an IVIS spectrum with imaging parameters set to: FOV D, 21.5 cm, binning = 8, exposure = auto, and f/stop = 1. The 20 nm band pass filters were set to 500, 520, 540, 560, 580, and 600 nm for quantification of bioluminescent signals required by the spectral unmixing software. The stage was heated to 37°C and a series of images acquired at 10 and 20 min post-*i.p.* injection of the substrates to determine the timing for maximal signal output. For sequential imaging of FZ and FFZ, the tumor-bearing mice were first injected *i.p.* with FZ and the bioluminescent signal captured the aforementioned band-pass filter set. Once the imaging session for FZ substrate was completed, clearance of the substrate was monitored after approximately 24 h by performing a pre-scan to access the absence of the signal. Then, FFZ was injected *i.p.* and BLI acquired. Bioluminescent signals were then quantified by spectral unmixing.

Spectral analysis and spectral unmixing of the *in vivo* images were performed by drawing ROIs with Living image software (PerkinElmer, version 4.5.1). For guided spectral unmixing, bioluminescent signals were recorded from tumors consisting of a pure, single-color BRET reporter cell populations following addition of each respective appropriate substrate. Once these single-color libraries were built, the relevant library spectra were then used to distinguish each BRET reporter contribution in heterogeneous dual- and triple-color multiplex tumors using the Living Image software. The spectral properties for each BRET reporter were drawn and quantified using the spectral unmixing algorithm.

METHOD DETAILS

Plasmid construction and stable cell line generation

Cloning of these constructs began with the linearization of the *pLenti-CMV-MCS-GFP-SV-puro* (Addgene #176837 from Odgren Lab, RRID: Addgene_73582) backbone with *Xba*I and *Bam*HI (NEB) restriction enzymes. Constructs containing the target Nanoluciferase (NanoLuc) fluorophore conjugate sequences were PCR amplified to create the cassette that included: the NanoLuc-fluorophore sequence, the appropriate restriction sites (*Xba*I and *Bam*HI), and an epitope FLAG tag for downstream protein quantification. The ligation product resulting from these components was subsequently introduced into STBL3 competent cells, followed by growth on agar plates supplemented with ampicillin. Multiple clones were selected for sequencing from which a singular positive clone was chosen for stocks and future experiments.

Stable cell lines were generated using a previously established viral transduction protocol.[47] High passage (>p100) UM-HMC-1 cells (RRID: CVCL_Y473) expressing the fusion reporter were maintained under 0.5 μg/mL of puromycin selection. Fresh cells were thawed after 15 passages. Growth media was composed of DMEM (Gibco ref# 11965-092) + 10% FBS (Premium Select; Atlanta Biologicals) + 20 ng/mL hEGF (Sigma cat# E9644) + 400 ng/mL hydrocortisone (Sigma cat# H088) + 5 μg/mL insulin (Sigma cat# 91077C) + 1× PSG (Gibco ref# 10378-016) + 1× Glutamax (Gibco ref# 35050-061) + 1× HEPES (Corning ref# 25-060-CI) + 1× Sodium Pyruvate (Gibco ref# 11360-070).

Western blotting

Whole cell lysates were prepared by lysing cells in a buffer consisting of 250 mM NaCl, 50 mM Tris (pH 7.4), 50 mM NaF, 0.1 mM $NaVO_4$, 5 mM EDTA, and 0.1% Triton X-100, supplemented with protease and phosphatase inhibitors. The lysates were then quantified for total protein concentration using the BCA assay (Thermo Scientific, cat# 23225). Approximately 20–30 μg of total protein was loaded onto a 8–20% gradient gel for SDS-PAGE and subsequently transferred onto a 0.2 μm nitrocellulose membrane (GE Healthcare Life Sciences, cat# 10600011). The loading of the protein was performed at 100 v for 15 min followed by 140 v for 1 h. The transfer was performed at a constant current of 400 mA for a minimum of 2 h. The membranes were then blocked with PBS-Tween containing 5% milk for 1 h at room temperature followed by a set of two PBS-T washes. Primary antibody incubation was carried out overnight at 4°C using monoclonal anti-FLAG HRP conjugated antibody (1:1000, Cat. #A8592; Millipore-Sigma, RRID: AB_439702) and anti-β-actin antibody (1:1000, cat# A1978; Millipore-Sigma, RRID: AB_476692) diluted in PBS-T. After washing with PBS-T, the membranes were incubated for 1h with rabbit anti-mouse IgG (H + L) (1:10 000, cat# 31450 ThermoFisher, RRID: AB_228427) secondary antibody at room temperature. Protein bands were visualized using Clarity ECL (Bio-Rad, cat# 170–5060) and imaged with the ImageQuant LHS4000 (GE) imaging system.

Spectral emission profiles

Nanoluciferase substrates

Furimazine (FZ) was sourced from Nano-Glo Luciferase Assay kits (Promega cat# N1130) and stored according to the manufacturer's instructions. Nano-Glo assay substrate is comprised of 5 mM FZ dissolved at 1.91 mg/mL in 85% ethanol and 15% glycerol. For *in vivo* experiments, 100 uL of a 1:20 dilution (250 μM) of this Nano-Glo assay substrate was prepared fresh with sterile DPBS (Corning, ref# 21-031-CV) prior to administration of each animal. Fluorofurimazine (FFZ) was directly provided in a purified, lyophilized cake from Promega Biosciences, LLC. To reconstitute a lyophilized cake of fluorofurimazine (FFZ) into 125 nmol solution, begin by adding 480 μL of room temperature (RT) double-distilled water directly onto 4.6 μmol lyophilized cake (Promega, now offered as cat# N4100). Following this initial dissolution, 1.82 mL of room temperature DPBS (Corning, ref# 21-031-CV) was added to the mixture. If clarification is needed due to undissolved particles, a brief centrifugation may be employed. The final 2 mM stock solution is then stored at −20°C as 20 μL aliquots to prevent repeated thaw cycles of the substrate.

Cytation 5-based monochromator detection

Cells were passaged at 80–90% confluency and 10,000 cells (cell density determined on DeNovix CellDrop) were seeded per well of a white, opaque, 96-well plate (Corning cat# 3916). concentrations on a Cytation5 plate reader (Biotek). Following seeding in 100 μL of full media, 100 μL of Furimazine (Promega cat# N113B) or Fluorofurimazine (provided by Promega) were added to a final concentration of 4 μM or 20 μM per well. The plate was then shaken for 5 s and the emission spectrum was obtained from 350 nm to 650 nm with integration time of 2 s at a step size of 5 nm. Substrate was prepared fresh for every 4 wells to prevent it from crashing out before addition to each well.

IVIS filter-based detection

Cells were passaged at 80–90% confluency and 30,000 cells were seeded per well of a white, opaque, 96-well plate. A 2× concentration of substrate in 100 μL is supplemented to each well of the plate followed by mixing with a pipette of the cell-substrate suspension. The plate was then imaged with 6 filter sets, each spanning 20 nm (band-pass filter sets used included: 500, 520, 540, 560, 580, and 600 nm). Photon flux values for all reporters are obtained from each of the 6 images corresponding to the 6 filters that are used for unmixing.

Kinetic decay curves

Kinetic curves were generated by seeding 10,000 cells in a white, opaque, 96-well plate and imaging 24 h later using the luminometer onboard the Cytation5 after the addition of 20 μM of substrate. Data points were taken in 5–8 s intervals between 30 min and 2 h, depending on the substrate concentration and the reporter being characterized.

In vitro cell proliferation

Growth rate of CeNLuc, GpNLuc, GeNL, YeNL, OeNL, and LumiScarlet reporters were determined by seeding 2,000 cells of each stable reporter line into individual wells of a black, clear bottom, 96-well plate (Corning cat# 3603) suspended in full media. Four plates were seeded per experiment. Each time point contained 8 technical replicates of each reporter. After every 24 h, one plate was decanted, and formalin fixed for 10 min followed by two PBS washes and a DAPI staining solution. Cell count was determined on the Cytation 5 plate reader.

In vitro cell imaging

Stable cell lines were passaged at 80–90% confluency and plated on a black, opaque, 96-well plate (Corning cat# 3917). Each well contained a total of 30K cells at a total volume of 100 μL in full media. Wells contained 100, 67, 33, or 0 percent of each reporter cell line.

Spectral libraries required for unmixing were created for each imaging session and for each unique substrate. The substrate at 2× final concentration was added prior to imaging of the plate on the IVIS Spectrum (PerkinElmer). The system then creates 3 composite images corresponding to the contribution of light from each reporter. Light contribution from each individual reporter was then normalized to the total light output from all three images, for each individual well.

Flow cytometry

Time of excision of the tumors was influenced by two main factors: *1*) a single tumor in a mouse reaching the critical volume of 2000 mm^3 or, *2*) the mouse losing too much weight at a rapid rate. Following excision, the tumors were processed for flow cytometry with a cold protease digestion protocol. Briefly, surgically resect the tumor and place a >250 mm^3 chunk on ice in complete growth medium supplemented with 1:1000 dilution of 10mM Y27632 (ROCK inhibitor - Selleckchem cat# S1049) until ready to process. Place the tumor chunk in the middle of a p10 or 35 mm dish on ice and finely mince the tissue using a fresh razor/scalpel ∼30 s. Prepare 2.5 mL of dissociation buffer with ice-cold 1xHBSS to which is added 2.5 μL Y27632, 1.5 μL RNase Inhibitor, 150 μL DNase I (Sigma cat# 11284932001), and 100 μL Bacillus licheniformis cold protease (Sigma cat# P5380). Add 500 μL of dissociation buffer to the plate containing the minced tumor, carefully rinse the dish to recover the tissue, and transfer to a fresh RNase/DNase free tube. Cut the tip of a p1000 pipette tip (∼1 cm from the end at an oblique angle to maximize aperture size) and triturate the tumor mix 20 times. Vortex 5 times in short 2 s bursts and place the tumor/dissociation mix on a rotator at 45 rpm inside a 4°C fridge. Remove and triturate the samples 10–20 times every 5 min and repeat this five time (25 min total). At the end of the first 25 min take a 10 μL of the sample and check under the microscope to ensure that ∼50% of the suspension is single cells with >95% viability. Next, use a 16-gauge needle to triturate the sample 15 times and place the tube back on the rotator for 5 min, then use an 18-gauge needle to triturate the sample 10 times and place the tube back on the rotator for 5 min, and lastly use 23.5-gauge needle triturate the sample 5 times and place the tube back on the rotator for 5 min. At this stage there should be a near 90–100% single cell population with > 90% cell viability. Filter the dissociated tumor solution through a 70 μm filter into a 50 mL conical. Wash the tube with 5 mL fully supplemented media to maximize recovery and filter. Pass an additional 5 mL media through the filter to maximize cell recovery and spin down the cells at 1500 g for 5–7 min. Prepare 1 mL of dissociated cell resuspension buffer with 975 μL of complete growth medium supplemented with 1 μL Y27632 and 25 μL DNase I. Resuspend cells in ∼1 mL of the dissociated cell resuspension buffer and count cells. Single cell samples run on Aurora (Cytek) instrumentation at UNC Core Facilities. FCS files were analyzed with FlowJo v10.8 software (BD Life Sciences, RRID: SCR_008520). Standard gating for single cell exclusion was performed on FSC-A versus FSC-W and SSC-A versus SSC-W. Live cells were determined via size exclusion for these runs. Single color tumors and non-transfected tumors were used as controls to set spectral unmixing controls to reduce off target auto-fluorescence and alleviate any loss of signal within animal transplant samples. Full spectra were exported per single color and non-transfected tumor samples, all remaining samples were exported as unmixed and used in downstream analysis.

QUANTIFICATION AND STATISTICAL ANALYSES

Statistical analyses were performed with GraphPad Prism (version 9, RRID: SCR_002798) using Student's t test, one-way ANOVA or two-way ANOVA where applicable. Data are presented as mean ± SD or mean ± SEM as indicated in the figure legends.